

# Computer Modeling of Ionic Micelle Structuring in Thin Films

Andrij Trokhymchuk,<sup>†,‡</sup> Douglas Henderson,<sup>†</sup> Alex Nikolov,<sup>§</sup> and Darsh T. Wasan<sup>\*,§</sup>

Department of Chemistry and Biochemistry, Brigham Young University, Provo, Utah 84602,  
and Department of Chemical Engineering, Illinois Institute of Technology, Chicago, Illinois 60616

Received: April 23, 2002; In Final Form: October 15, 2002

The phenomenon of layering of like-charged particles (ionic surfactant micelles or other colloidal particles) between two plane-parallel film surfaces and the evolution of in-film particle structuring are studied using the canonical Monte Carlo method combined with a simulation cell containing both the bulk solution and the film region. The simulations are performed using an effective one-component fluid potential model that incorporates micelle hard-core repulsion and both the screened Coulomb electrostatic interaction and the entropic contribution due to the discrete nature of the solvent and finite size of electrolyte ions. The proposed potential model is applied to mimic the properties of surfactant micelle solutions in the bulk and under film confinement. The effects of surfactant concentration and film thickness on the in-film micellar structuring phenomenon are analyzed. The relation of obtained results to experiments on stratifying sodium dodecyl sulfate micellar films is discussed.

## 1. Introduction

The phenomenon of layering, i.e., the stepwise stratification in thin liquid films formed from solutions of surfactant micelles and other colloidal particles, has received considerable attention because thin films are used as a tool to probe the structural forces in concentrated colloidal suspensions.<sup>1–11</sup> It has been observed that these films stratify, become thinner, in a regular stepwise manner. The height of the stepwise thickness transition is nearly constant and has been associated with the effective particle (or micelle) diameter.<sup>10,11</sup>

Our previous theoretical works dealt with the modeling of charge-stabilized (hard-sphere) particles confined between two close flat walls, i.e., thin films. Both the experiments<sup>1–11</sup> and theoretical studies<sup>12–14</sup> showed that as a result of the confinement, the particles formed layers in the direction parallel to the film surfaces, and as the particle concentration in bulk increases, an ordered quasi-two-dimensional structure within the layers is formed. The in-layer structural transition depends on the film thickness and on the position of the layer inside the films. The film stratification (or layering) is a manifestation of the long-range structural (non-DLVO) forces acting between film surfaces and offers a new mechanism for stabilizing colloidal dispersions. The role of the structural forces in the stability of macrodispersions such as foams, emulsions, and particle suspensions has been demonstrated by us recently.<sup>15–18</sup>

In the present paper we are interested in the layering phenomenon in confined charged colloids such as ionic micelles and the evolution of the layered structure with the changes in film thickness. Our study is based on the one-component fluid (OCF) model approximation.<sup>19</sup> Usually, according to this approach, the micellar solution is viewed as an effective one-component fluid of macroions (i.e., micelles) interacting via the

electrostatic forces by means of the screened Coulomb (SC) potential.<sup>20</sup> The effects of the solvent and simple (electrolyte) ions are presented, incorporated in the SC potential via a continuum approximation; i.e., they are incorporated in determining the screening length only. The main goal of the present study is to take into account both the finite size of the simple (electrolyte) ions and the discrete nature of the solvent that result in the entropic forces, i.e., the excluded volume effects. To achieve this goal the OCF model approximation in our study is based on the effective interaction between two macroions that includes both electrostatic and entropic interactions. In our treatment, the entropic interaction is additive to the electrostatic screened Coulomb potential and is evaluated within the hard-sphere (HS) fluid approximation. Therefore, the proposed model is a hard-sphere plus screened Coulomb one-component fluid abbreviated as the HS/SC/OCF model.

The only electrostatic counterpart of the one-component fluid approach to colloidal solutions, i.e., the SC/OCF model, has been considered by many authors.<sup>21–25</sup> In the most recent study, Pollard and Radke<sup>25</sup> employed the SC/OCF approach in their density functional modeling of structure and forces in thin micellar films. Presuming the micelles to have a hard-core diameter and to interact with each other via a screened Coulomb potential, these authors found that the SC/OCF model captures qualitatively the essential features of the properties of the micellar films if the concept of the effective micelle size (micelle hard-core diameter plus the Debye atmosphere) is used. On the other hand, the hard-sphere counterpart of the HS/SC/OCF model, i.e., effective one-component hard-sphere fluid (HS/OCF) model, has been studied recently<sup>26–28</sup> as well. It has been shown that the HS/OCF model accounts satisfactorily for both the bulk (structure and phase equilibria) and the confinement (local ordering) conditions in a true binary hard-sphere mixture. Thus, the proposed HS/SC/OCF model has a solid theoretical foundation because both complementary parts, i.e., screened Coulomb and depleted hard-sphere models, are well founded.

The entropic forces, which are taken into account in the present study and result from both the finite size of the simple

\* Corresponding author. E-mail: wasan@iit.edu. Phone: (312)5673001. Fax: (312)5673003.

<sup>†</sup> Brigham Young University.

<sup>‡</sup> Permanent address: Institute for Condensed Matter Physics, National Academy of Sciences of the Ukraine, Lviv 11, Ukraine.

<sup>§</sup> Illinois Institute of Technology.

**TABLE 1: Experimental Data for Micellar Surfactant Solutions<sup>1</sup>**

| surfactant concn,<br>$C$ (mol/L) | Debye length,<br>$1/\kappa$ (nm) | micellar volume<br>fraction, $\eta_m$ |
|----------------------------------|----------------------------------|---------------------------------------|
| 0.03                             | 3.20                             | 0.013                                 |
| 0.10                             | 2.45                             | 0.051                                 |

(electrolyte) ions and from the discrete nature of the solvent, will allow us to verify on the quantitative level the modeling trends with experimental observations. Monte Carlo simulation data for the HS/SC/OCF model reported in the present study are generated within the canonical ensemble technique combined with a simulation cell containing both the bulk solution and the film region.

## 2. Some Experimental Facts

Thinning foam films formed from sodium dodecyl sulfate (SDS) surfactant solutions is the prototype of our modeling in this study. For such surfactants, the micelles are formed beyond the critical micelle concentration (CMC), which is 0.008 mol/L in the case of SDS. The micelles that are formed are fairly narrowly dispersed in size and are charged with the net charge being less than the aggregation number. Reiss-Hussen and Luzzati<sup>29</sup> used a low-angle X-ray technique and have established that there exists a concentration range (0.03–0.10 mol/L) when the micelles are spherical (the micelle sphere-to-rod shape transition occurs at a concentration of 0.25 mol/L). The aggregation number of spherical micelles is 67, and the micelle (hard-core) diameter has a value of 4.8 nm and does not depend on the surfactant concentration (in this concentration range).

The micelles are in equilibrium with SDS monomers, which are dissociated into  $\text{Na}^+$  and  $\text{DS}^-$  ions in the solution. In this way, the ionic SDS monomers and aqueous solvent serve as the simple electrolyte medium for micelle units. The micelles are partially dissociated, and the degree of dissociation in a concentration range from 0.03 to 0.08 mol/L was measured and found to be around 27%,<sup>30</sup> i.e., 18 charges per micelle. For this reason, the mean concentration of  $\text{Na}^+$  ions in the solution is higher than the mean concentration of  $\text{DS}^-$  ions. However, to characterize the electrolyte, the Debye length,  $\kappa^{-1}$ , which is calculated from the definition

$$\kappa^2 = \frac{4\pi e^2 N_A}{10^3 \epsilon k T} (C_{\text{Na}} + C_{\text{DS}}) \quad (1)$$

can be used. In eq 1,  $N_A$  is Avogadro's number,  $k$  is the Boltzmann constant,  $T$  is the temperature,  $\epsilon$  is the solvent dielectric constant,  $e$  is the charge of an electron (in CGS units), and  $C_{\text{Na}}$  and  $C_{\text{DS}}$  are the ionic concentrations (moles per liter). The concentration  $C_{\text{Na}}$  accounts for both the  $\text{Na}^+$  ions dissociated from the SDS monomers and from the micelles. The resulting concentration of micelle particles has been calculated using the Hartley model<sup>31</sup> assuming a spherical micelle shape and an aggregation number 67. From the concentration of micelles one can calculate the volume fraction,  $\eta_m$ , occupied by micelle particles. Table 1 presents the complete set of experimentally derived data<sup>1</sup> that are necessary input for modeling of micellar solutions of SDS surfactant.

## 3. Modeling of the Surfactant Micelle Bulk Solution

Definition and calculation of an effective pair potential is the crucial aspect in the OCF approach. Different routes to derive the expression for the effective interaction,  $U_{\text{mm}}^{\text{eff}}(r)$ , between two like-charged macroions in the presence of a simple

electrolyte have been considered because the classical DLVO potential was proposed by Derjaguin and Landau<sup>32</sup> and Verwey and Overbeek<sup>33</sup> in the 1940s. The recent attempts of Sogami and Ise,<sup>34</sup> Spalla and Belloni,<sup>35</sup> and others have been stimulated by experimental observations for colloidal suspensions<sup>36–39</sup> that seem to be inconsistent with the DLVO theory. All of these calculations are consistent at the level of Poisson–Boltzmann approximation but differ quantitatively and conceptually in the case when the size of the electrolyte ions is not negligible. Furthermore, in the present study we are aiming at an even more sophisticated case in which the size of the solvent molecules has to be taken into account. This task requires that the average distribution of the solvent molecules and electrolyte ions around the two fixed macroions must be accounted for. A route that directly utilizes this concept is based on the evaluation of the effective average interaction or potential of mean force,  $W(r)$ , via the macroion radial distribution function,  $g_{\text{mm}}(r)$ , using the definition

$$\frac{1}{kT} W(r) = -\ln g_{\text{mm}}^{\text{o}}(r) \quad (2)$$

The superscript “o” indicates that only two macroions are involved; i.e., statistically it means that the theoretical macroions should be in the limit of infinite dilution. The latter point is very important, as otherwise the correlations between a pair of fixed macroions are affected by many-body effects and  $W(r)$  will not be a true pair interaction. Moreover, the degree of success of eq 2 is concerned now with the modeling of supporting electrolyte that is used to calculate the radial distribution function,  $g_{\text{mm}}^{\text{o}}(r)$ , and with the approximations involved in these calculations.

### 3.1. Initial Many-Component Model of Micellar Solution.

The effective interaction between ionic micelles immersed in an aqueous electrolyte solution is dominated by electrostatic and solvation forces.<sup>40</sup> The electrostatic forces are determined by the number of charges carried by the micelles and by the concentration of supporting electrolyte solution. The solvation forces are promoted by the water-like solvent. The electrostatic effects between micellar macroions are described remarkably well (see, for example, ref 20) within the *primitive* model for supporting electrolyte: charged hard spheres in a continuum solvent of fixed dielectric permittivity. The simplest *nonprimitive* model for the supporting electrolyte that accounts for the solvation forces is charged hard spheres in a hard-sphere solvent with the same dielectric permittivity. With regard to the subject of the present study, the complete model that involves the macroions (i.e., micelles) is formulated as follows: two large charged hard spheres of diameter  $d_m = 2R$ , bearing a fixed charge  $eZ_m$ , are immersed in a fluid (low-charge electrolyte solution) consisting of neutral hard spheres (solvent molecules) with density  $\rho_s$  and diameter  $d_s$  plus two species of charged hard spheres (cations and anions) with charges  $eZ_+$  and  $eZ_-$ , densities  $\rho_+$  and  $\rho_-$ , and diameters  $d_+$  and  $d_-$ . Because the number density of the solvent molecules dominates that of the ions, for simplicity we assume  $d_+ = d_- = d_s \equiv d_0$ , i.e., all small discrete entities that form the simple (supporting) electrolyte solution have the same geometrical dimensions. Resulting direct interparticle interaction potentials in such a model system then are the sum of the corresponding hard-core repulsions and the bare electrostatic interactions that are screened with a macroscopic dielectric permittivity of the solvent subsystem,  $\epsilon$ .

**3.2. Mean Spherical Approximation.** To calculate the radial distribution function between micellar spheres,  $g_{\text{mm}}^{\text{o}}(r)$ , we turn

to the mean spherical approximation (MSA) solution of the Ornstein–Zernike (OZ) equation for the model in question.<sup>41</sup> Vericat and Blum<sup>41</sup> have reported the OZ/MSA solution for a very general case of ion–dipole model: an arbitrary number of ionic species with arbitrary charges and hard-core diameters plus a single species of dipole hard spheres that serve as a solvent. In our previous publications<sup>42–44</sup> we addressed the MSA solution for the problem of two macroions in the ion–dipole electrolyte, and the results for the pair correlation function,  $h_{mm}^{o,MSA}(r) = g_{mm}^{o,SA}(r) - 1$ , were presented and discussed. In particular, it was pointed out that for a linearized theory, such as the MSA, the logarithm in eq 2 should be linearized and replaced by  $h_{mm}^{o,MSA}(r)$ . Thus, the potential of mean force between two macroions in an electrolyte solution can be calculated as follows:<sup>43,45</sup>

$$\frac{1}{kT}W(r) = -h_{mm}^{o,MSA}(r) \quad (3)$$

This is the approximation that we will use in the present study to define an effective interaction between two like-charged macroions.

Following the MSA solution,<sup>41–44</sup> the pair correlation function,  $h_{mm}^{o,MSA}(r)$ , consists of a hard-sphere term,  $h_{HS}^{o,PY}(r)$ , obtained within the Percus–Yevick (PY) approximation,<sup>45</sup> and an electrostatic term,  $\Delta h_{EL}^{o,MSA}(r)$ . The hard-sphere and electrostatic contributions are additive in the MSA, i.e.,

$$h_{mm}^{o,MSA}(r) = h_{HS}^{o,PY}(r) + \Delta h_{EL}^{o,MSA}(r) \quad (4)$$

The contribution,  $h_{HS}^{o,PY}(r)$ , depends on the total (small ions plus solvent molecules) volume fraction occupied by the supporting electrolyte solution,  $\eta_0 = (\pi/6)(\rho_i + \rho_s)d_0^3$  with  $\rho_i = \rho_+ + \rho_-$ . The electrostatic term,  $\Delta h_{EL}^{o,MSA}(r)$ , depends on both the volume fraction,  $\eta_0$ , and the inverse Debye length,  $\kappa$ . Therefore, from eqs 3 and 4, we note that the effective average interaction between two micellar macroions immersed in an electrolyte solution consists of two essential contributions which originate from (i) the discrete nature of the solvent molecules and finite size of electrolyte ions and (ii) the electrostatic nature of electrolyte.

**3.3. Effective Pair Potential.** As a result, the effective potential between a pair of micelle particles,  $U_{mm}^{eff}(r)$ , can be presented in a form

$$U_{mm}^{eff}(r) = \begin{cases} \infty & r \leq d_m \\ W(r) \equiv u^{EN}(r) + u^{EL}(r) & r > d_m \end{cases} \quad (5)$$

where the symbol  $\infty$  in the first row accounts for the hard-sphere repulsion between micelle cores of the diameter,  $d_m$ .

The first term in the second row,  $u^{EN}(r)$ , represents the excluded volume interactions induced by the entropic forces and is related to  $h_{HS}^{o,PY}(r)$  through eqs 3 and 4. This is purely a hard-sphere excluded volume contribution and is present even in the uncharged system. In the micellar solutions entropic forces arise between a pair of large micellar spheres dispersed in a suspension of small spheres that represent the discrete solvent and the nonzero diameter electrolyte ions of the total volume fraction,  $\eta_0$ . Initially, the importance of entropic forces has been shown by Asakura and Oosawa<sup>46</sup> through the so-called depletion attraction between the surfaces of two large bodies if the separations between them is less than one diameter of the smaller solute molecules. Later, the role played by entropic forces has been intensively studied and discussed in the literature by different groups of researchers.<sup>45,47–50</sup> As a result, in addition

to the depletion attraction, a repulsive barrier at larger separations and beyond that a secondary minimum have been found.<sup>45,48</sup> At present it is well-recognized<sup>49,50</sup> that entropic forces between two large particles, depending on the density of the small particles, could extend to separations greater than one diameter of the small particles by means of the so-called structural forces. Thus, the entropic contribution to the effective interaction between two large micellar spheres is composed of two terms and can be evaluated in the form<sup>49</sup>

$$u^{EN}(r) = \begin{cases} \phi^{dep}(r) & d_m < r \leq r^* \\ \phi^{str}(r) & r > r^* \end{cases} \quad (6)$$

Here  $\phi^{dep}(r)$  and  $\phi^{str}(r)$  are the depletion (analogue of that found by Asakura and Oosawa<sup>46</sup>) and structural parts, respectively, of the entropic interactions. Although the depletion and structural interactions are of the same (entropic) origin, their extension range and intensity are quite different. This is reflected in their functional (versus separation) representation as well. At low values of the volume fraction of the small particles,  $\eta_0$ , the depletion part of the entropic potential is well described by the Asakura and Oosawa result<sup>46</sup> whereas the structural part is set to be zero. However, with an increase in the small particles packing fraction the depletion part exhibits a repulsive barrier and to a good approximation,  $\phi^{dep}(r)$  can be described by<sup>49</sup>

$$\frac{1}{kT}\phi^{dep}(x) = \left(\frac{d_m + d_0}{2d_0}\right)(a + bx + cx^2 + dx^3) \quad (7)$$

with coefficients that depend on the volume fraction occupied by the small particles:<sup>49</sup>

$$\begin{aligned} a &= -2.909\eta_0 \\ b &= 6.916\eta_0 - 4.616\eta_0^2 + 78.856\eta_0^3 \\ c &= -4.512\eta_0 + 15.860\eta_0^2 - 93.224\eta_0^3 \\ d &= -\eta_0 \exp(-1.734 + 8.957\eta_0 + 1.595\eta_0^2) \end{aligned} \quad (8)$$

The structural part at higher volume fractions of the small particles is of oscillating nature, i.e., structural forces can be either repulsive or attractive, and their contribution to the entropic interaction is described well by<sup>43,49,50</sup>

$$\frac{1}{kT}\phi^{str}(x) = u_0 \cos(\omega_0 x + \varphi_0) \exp(-\kappa_0 x) \quad (9)$$

where again the coefficients depend on the density of small particles. However, only the frequency and decay coefficients,  $\omega_0$  and  $\kappa_0$ , respectively, have been parametrized so far:<sup>43,49,50</sup>

$$\begin{aligned} \omega_0 &= 4.4516 + 7.10586\eta_0 - 8.30671\eta_0^2 + 8.29751\eta_0^3 \\ \kappa_0 &= 4.78366 - 19.64378\eta_0 + 37.37944\eta_0^2 - 30.59647\eta_0^3 \end{aligned} \quad (10)$$

The amplitude and phase coefficients,  $u_0$  and  $\varphi_0$ , respectively, should be specified for a particular density of the small particles. Quite arbitrarily, we took the volume fraction of the small hard spheres to be  $\eta_0 = 0.30$ ; this is a typical value for an aqueous solvent. The amplitude and phase coefficients in eq 9 that correspond to this density are  $u_0 = -0.46(1 + d_m/d_0)$  and  $\varphi_0 = -0.65$ .

The distance parameter,  $x$ , in eqs 7 and 9, is related to the separation between the centers of two large spheres,  $r$ , as follows:  $x = (r - d_m)/d_0$ , i.e.,  $x$  is the separation between the



outer surfaces of two micellar particles. The distance  $r = r^*$  in eq 6 defines the position between the centers of two large particles where the depletion and structural forces are matched. This position lies within the separation of one diameter of the small particles between the outer surfaces of two large spheres and depends sensitively on the density of the small particles.<sup>49</sup> In our particular case when the density of small particles is fixed at value  $\eta_0 = 0.30$ , parameter  $r^*$  is  $1.0789d_m$ .

Finally, the second term,  $u^{\text{EL}}(r)$ , in the bottom row of eq 5 is the electrostatic contribution to the effective interaction between two micellar macroions. To simplify our analysis, we will evaluate the contribution of the electrostatic forces to the potential energy in a simplified form that is similar to that suggested by Blum and Høye<sup>51</sup> and is widely used<sup>22–25</sup> to model the bulk micelles:

$$\frac{1}{kT} \mu_{\text{mm}}^{\text{EL}}(r) = \frac{Z_m^2 \lambda_B}{(1 + \kappa d_m)^2} \frac{e^{-\kappa(r-d_m)}}{r} \quad r > d_m \quad (11)$$

$\lambda_B = e^2/(4\pi\epsilon_r\epsilon_0 kT)$ , is the Bjerrum length and  $\kappa$  is the inverse Debye screening length defined by eq 1.

In principle, we could utilize a more accurate expression for electrostatic contribution incorporating, for example, dipole alignment and ion correlation effects;<sup>44</sup> but we felt that the screened Coulomb level is capable of capturing the physical aspects we wish to address in this study. Besides, the appropriate analytical equations for electrostatic contribution to the effective interaction between charged colloids, which is an important attribute of computer simulation studies, are not available for the moment.

**3.4. Modeling of the Film Interfaces.** The model micellar film can be formed by immersion of a pair of molecularly smooth parallel confining surfaces into the bulk of a micellar solution. To proceed with modeling, we must define the interactions introduced by the presence of film surfaces. Usually, the theoretical studies dedicated to the films formed by surfactant micelles assume that the film surfaces are charged.<sup>21–25</sup> Consequently, the form of interaction potential between an individual micellar particle and a film surface is obtained as the limit of the DLVO potential between two charged particles when the second particle becomes infinitely large and uniformly charged with the finite charge surface density  $\sigma$ . In this case  $\sigma$  becomes a new interaction parameter that affects the film stability. In practice, the molecularly smooth mica plates or the air–water interfaces could serve as a prototype of film surfaces. When these previously uncharged surfaces are found to be in an ionic surfactant solution, indeed, they can come charged by the adsorption (binding) of ionic surfactant below the CMC and the surfactant bilayers and/or surfactant micelles above it.<sup>9,40–52</sup> Whatever the charging process, the final surface charge is balanced by an equal but oppositely charged regions of the Stern and diffuse electric double layers.<sup>40</sup> We are interested in a surfactant concentration far above the CMC. Because micellar surfactant solution in the present study is modeled within the OCF approach, i.e., the surfactant ions as well as the counterions are not considered implicitly, we assume that the film surfaces initially are uncharged, allowing them to become charged self-consistently by the adsorption of charged micelle particles. In such a way, on one hand, we simplified the modeling to not introducing an extra parameter  $\sigma$ . On the other hand, the micellar particles are determined to play a role in the film stability.

Proceeding in this way and trying to be consistent with the modeling of the bulk solution, we found the effective interaction between micelles and film surfaces (walls),  $U_{\text{mw}}^{\text{eff}}$ , consists of an

entropic contribution originating from the discrete nature of the solvent. The latter is similar to that between two micellar particles,  $u^{\text{EN}}(r)$ , but with a factor of 2, according to the Derjaguin approximation<sup>40</sup> that relates the interaction between two large spheres and that between a large sphere and planar wall.

$$U_{\text{mw}}^{\text{eff}}(z) = \begin{cases} \infty & z < z_{\text{left}} \text{ or } z < z_{\text{right}} \\ 2u^{\text{EN}}(r) & z_{\text{left}} \leq \text{ or } z \leq z_{\text{right}} \end{cases} \quad (12)$$

Here  $z_{\text{left}}$  and  $z_{\text{right}}$  are the positions of the left and right film surfaces, respectively. The variable  $z$  is the distance from the center of the micelle macroion to the plane of the slit. The closest approaches of the center of micelle macroions to the impenetrable surfaces are therefore  $z = z_{\text{left}} + d_m/2$  and  $z = z_{\text{right}} - d_m/2$ .

#### 4. Computer Simulations

An important prerequisite for the computer simulation study of the liquid adsorbed into a two-surface (film) confinement under controlled thermodynamic conditions is the method used to establish equilibrium between the liquid in a film region and that in a contiguous bulk solution (reservoir). In our case, this means that a model micellar solution confined between two surfaces must be in equilibrium with a reservoir of the same model fluid at prescribed bulk density conditions (solvent density,  $\rho_s$ , electrolyte concentration characterized by the inverse Debye length,  $\kappa$ , and micellar concentration,  $\eta_m$ ) or, equivalently, a prescribed value of the chemical potential,  $\mu(\rho_s, \kappa, \eta_m)$ . Such a system setup corresponds also to the laboratory conditions when, usually, the pressure in the reservoir is fixed at atmospheric pressure, allowing the volume of the reservoir to fluctuate. Widely used techniques to simulate such systems are the grand-canonical or Gibbs ensemble Monte Carlo methods.<sup>53,54</sup> In both schemes, the chemical potential and the volume of the system are maintained constant, whereas the number of particles is allowed to fluctuate around a value specified by the chemical potential through particle insertion and deletion. Consequently, the grand-canonical or Gibbs ensemble methods simulate an equilibrium without explicitly connecting the film and the reservoir. As an alternative, Gao et al.<sup>55–57</sup> have proposed combining canonical ensemble simulations with a computational cell containing both bulk (reservoir) and confined fluid regions. Obviously, the final results should not depend on the method although, depending on the type of the system simulated, an advantage in using one method or the other may exist.

Recently, using a scheme similar to that of Gao et al.,<sup>55–57</sup> we have been able to study the properties of a pure aqueous film as a function of film thickness.<sup>58</sup> Mainly due to this, in the present study we use the same approach, i.e., the canonical Monte Carlo method where the film region and a bulk solution (reservoir) are connected within the same simulation cell in the way that is sketched in Figure 1. The basic rectangular simulation box has dimensions  $L_x \times L_y \times L_z = 30 \times 10 \times 30$  (in the units of the micelle hard-core diameter,  $d_m$ ). Periodic boundary conditions are applied in all three directions. With the exception of the regions of two rectangular subcells (denoted as “left subcell” and “right subcell” in Figure 1) that mimic the macroscopic objects (air bubbles, oil droplets, mica plates, etc.) that form the film, the system is filled with micellar macroions. Left and right subcells each are confined by three structureless hard walls. Two of them that are perpendicular to the  $x$ -direction are necessary to prevent micellar particles from entering into the subcell’s interior from the bulk side. The third,  $XY$  planes of each subcell, which are perpendicular to the  $z$ -direction,

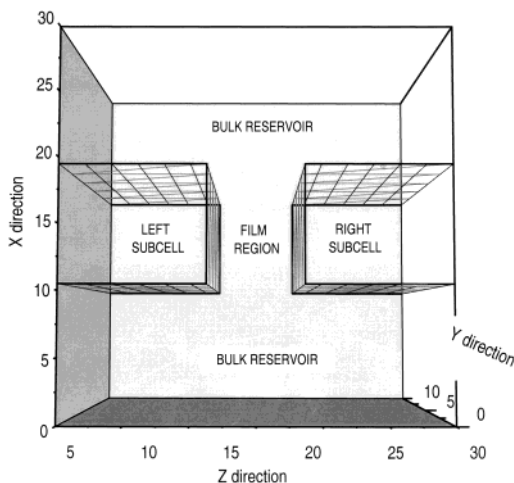


**Figure 1.** Sketch of the basic cell employed in canonical Monte Carlo simulations. The cell has the form of a rectangular box of dimensions  $L_x \times L_y \times L_z = 30 \times 10 \times 30$  (in the units of the micellar diameter,  $d_m$ ) with the coordinate origin at  $x = y = z = 0$  and contains both bulk and film regions. Two bulk regions are the parts of the same reservoir that is connected with the film region formed in the space between two empty subcells. Each subcell is confined by three planes that are necessary to prevent particles from entering into the subcell's interior. The XY planes of each subcell, perpendicular to the z-axis, form the slit pore (slitlike film). The film midplane is located at  $z/d_m = 15$ .

represent the actual film surfaces and form the slit pore (slitlike film) of thickness  $H$ . The film midplane is located at  $z = 15d_m$ . The film surfaces are movable and for each thickness,  $H$ , are fixed at  $z = z_{\text{left}}$  and  $z = z_{\text{right}}$  where  $z_{\text{left}}$  and  $z_{\text{right}}$  are equal to  $15 \pm H/2$ , respectively. With periodic boundary conditions, these settings result in a rectangular cell that is continuous along the y-direction.

The total energy of the system is the sum of the contributions from the micelle–micelle, micelle–surface, and surface–surface interactions. The potential model for the micelle–micelle interaction,  $U_{\text{mm}}^{\text{eff}}$ , and for the micelle–surface interaction,  $U_{\text{mw}}^{\text{eff}}$ , have been defined in a previous section and are specified by eqs 5 and 12, respectively. The film surfaces in the present study are neutral hard walls; i.e., the internal energy of the system is irrelevant to the surface–surface interaction.

According to eqs 5 and 12, both micelle–micelle and micelle–surface interactions contain an entropic component that includes a strong short-ranged depletion attraction at separations on the order of the dimension of the solvent molecules. In general, depending on the strength of electrostatic repulsion, this attraction could (or could not) lead to the particle–particle coagulation or strong particle–wall adsorption (binding). This feature of the micellar model with entropic forces makes the simulation procedure similar to some extent to that for chemically associating fluids,<sup>59,60</sup> where it was suggested that the efficient simulation scheme to displace the particles should depend on the details of the potential model. In particular, it has been found that a standard displacement scheme to move the particles uniformly on the unique interval from 0 to  $d_m$  ( $d_m$  is the micelle particle diameter) is an inefficient because it produces many displacements of length  $d_m$  and a very few small displacements of length  $d_0$  ( $d_0$  is the suspended molecule diameter). Therefore, very few trial configurations are generated in which the particles explored various positions in the depletion potential well. In accordance with this, the displacement scheme to move the particles that we applied in this study, consists of two steps, namely a large displacement on the interval  $(0, r_{\text{max}})$  and a small displacement on the interval  $(0, r'_{\text{max}})$ . Necessarily,

the variable  $r_{\text{max}}$  is set to a value large enough (order of a few micelle hard-core diameters,  $d_m$ ) to allow the particle–particle or particle–film surface depletion binding and breaking. The small displacement,  $r'_{\text{max}}$ , is chosen to be on the order of a few solvent molecule diameters,  $d_0$ . Both displacement steps have been chosen from a uniform distribution in the interval  $(0, r_{\text{max}})$  and  $(0, r'_{\text{max}})$ , respectively, and were used with the same probability. The maximum values  $r_{\text{max}}$  and  $r'_{\text{max}}$  in each particular run were adjusted to produce a probability of acceptances in the range 10–30%.

The total number of micellar particles,  $N$ , used in the simulation depends on the surfactant concentration we are interested in. Additionally, for each fixed surfactant concentration the number of micelles varies slightly when the separation between film surfaces changes. Therefore, for each film thickness number  $N$  was adjusted to maintain the same bulk conditions (micellar particle bulk volume fraction). Depending on the film thickness the total number of particles was in the range  $N = 190 \pm 10$  at a low surfactant concentration and  $N = 620 \pm 30$  at a moderate surfactant concentration. Production Monte Carlo runs during which ensemble averages were collected consist of over  $10^8$  configurations, after discarding an initial equilibration run of at least  $10^7$  configurations. The criteria used for determining whether equilibration had been reached were the following: the symmetry of the density profiles on each side of the film midplane up to each film surfaces and the lack of any dependence of the film and bulk properties (with a standard deviation within 5%) on the length of simulation runs. The bulk radial distribution function and the density profiles,  $\rho(H, z)$ , were evaluated from histograms updated every  $2N$  configurations with a grid size  $0.01d_m$  (or equivalently,  $0.1d_0$ ).

## 5. Results and Discussion

Two systems discussed in the present study are determined by the two different volume fractions occupied by the micelles in a bulk phase, namely,  $\eta_m = 0.012$  and  $0.049$ . According to Table 1, these two volume fractions could be associated with the micellar solutions characterized by two different surfactant concentrations of 0.03 and 0.10 mol/L, which afterward are referred to as the micellar solutions of low and high surfactant concentrations, respectively. However, the reader should keep in mind that from the point of the present simulation studies this means that there are two different volume fractions of the micellar macroions in a bulk region of the simulation cell. We note that all results presented in this study mimic the aqueous solutions at room temperature,  $T = 298$  K. Consequently, the corresponding value of the Bjerrum length,  $\lambda_B$ , in eq 11 is 0.714 nm. The micelle particle to solvent molecule size ratio,  $d_m:d_0$ , that is necessary input to effective modeling of entropic forces, is chosen to be 10:1.

The main results are presented for the micelle charge number as large as 30 charges per micelle, i.e.,  $Z_m = 30$  although some simulations with lower values of  $Z_m$ , namely, 20 and 10 have been performed as well. Also we already mentioned, the volume fraction occupied by the supporting electrolyte (solvent plus simple electrolyte ions) is fixed at  $\eta_0 = 0.30$ .

**5.1. Two Micelles in an (Effective) Electrolyte.** We start our discussion by analyzing the forces acting between only two micellar particles. This is a hypothetical case for both theory and experiment; however, the forces acting between a pair of isolated particles is a key ingredient in the statistical mechanical description of the properties of the system. If a pair of micelles would be in a vacuum, then the forces acting between them

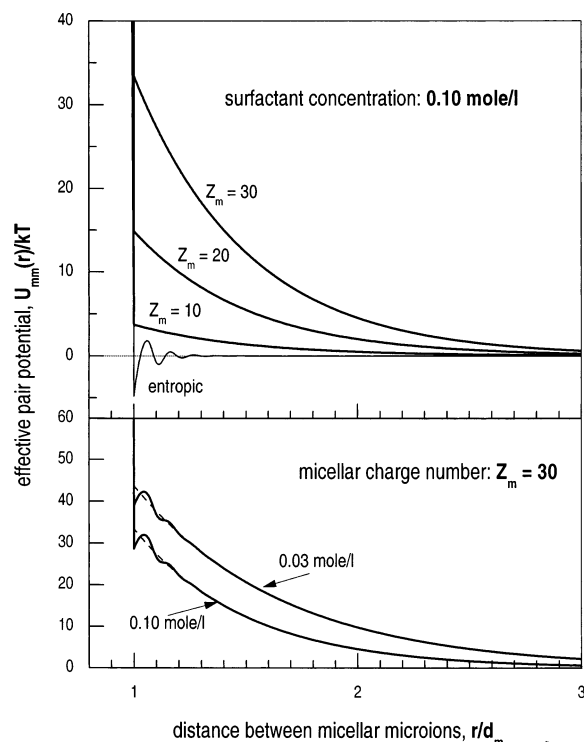


**Figure 2.** Effective pair interaction between a pair of isolated micellar particles. The upper part shows entropic contribution (thin solid line) and the three electrostatic DLVO contributions (thick solid lines) that correspond to three different micellar charge numbers as depicted on the figure. The bottom part shows the total interaction (thick solid lines) at both the low and high surfactant concentrations. The micellar charge number is fixed at 30 charges per particle. The thin dashed lines represent the DLVO interaction in these cases.

will be determined by the individual parameters of each particles only that for the present modeling are limited to the hard-core diameter,  $d_m$ , and micellar charge number,  $Z_m$ . In contrast, within a one-component fluid approach the pair interaction is effective and depends on the physical properties of a suspended subsystem. In the present study such properties include the concentration of surfactant electrolyte or Debye screening length,  $\kappa$ , the dielectric constant of the aqueous solvent,  $\epsilon$ , and the total (solvent plus electrolyte) volume fraction occupied by suspended subsystem. The first two parameters are the same as in DLVO theory and are responsible for the electrostatic forces. The last parameter is not accounted for within the DLVO theory and is responsible for the entropic forces. Assuming the volume fraction of the suspended subsystem is equal to zero (i.e., neglecting the discrete nature of electrolyte) eliminates the contribution of entropic forces and our model reduces to a DLVO-like model.

Figure 2a shows separately the electrostatic (DLVO-like) and entropic contributions to the effective interaction potential between two micellar macroions,  $U_{mm}^{eff}$ . The electrostatic contribution is repulsive and decays monotonically with distance, extending to a few diameters of micellar macroions. The intensity of the electrostatic repulsion depends strongly on the micellar charge number,  $Z_m$ . The range of electrostatic interaction is determined by the surfactant concentration: an increase in the surfactant concentration leads to a shortening of the range of the repulsion but at the same time affects (slightly increases) the strength of repulsion. In contrast, the entropic contribution is an oscillatory decay. It has repulsive and attractive parts with the periodicity of oscillations scaled by the geometrical dimensions of the suspended component. The entropic contribution

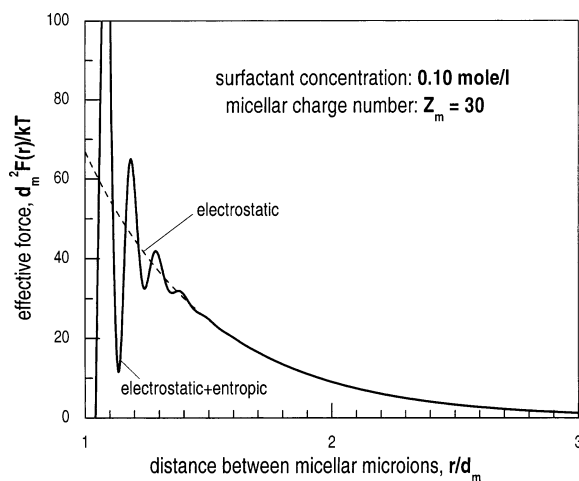


**Figure 3.** Effective force between two micellar particles that corresponds to the total effective interaction shown in the bottom part of Figure 2. Notations used for the lines are the same as in Figure 2.

vanishes when the separation distance between two micellar macroions exceeds the distance of four-to-five diameters of the suspended atomic entities (approximately 2 nm or less than half of a micellar hard-core diameter in the case of SDS surfactant micelle solutions). Because the number density of the solvent molecules dominates that of the electrolyte ions, we suppose that the entropic forces are not sensitive to the variations of the surfactant concentration. In what follows, the contribution of entropic forces to the effective interaction between two micelles has been evaluated in all our calculations at the conditions that correspond to a fixed volume fraction of suspended subsystem, namely, 30%, that is, of the order of typical volume fraction of aqueous solutions (solvent molecules plus salt ions).

The total effective interaction between two micelles immersed in an ionic surfactant solution in accordance with eq 5 is a sum of electrostatic and entropic contributions.  $U_{mm}^{eff}$  incorporates the characteristic features of both counterparts as can be seen from Figure 2b where both low and high surfactant concentrations are displayed. In particular, for both solutions we observe the oscillatory modulated repulsion at small separations between particles. An increase in a surfactant concentration raises the screening ability of the effective medium, which results in a reduction of the strength and shortening of the range of electrostatic repulsion.

An example of the force (derivative of the pair potential with respect to the separation) experienced by the two approaching micellar macroions is shown in Figure 3. The oscillatory decay part of the force profile reflects in an effective way the impact of the discrete nature of the solvent on interparticle forces. The structural component of entropic forces due to the solvent molecules modulates the repulsive electrostatic interactions so that it become oscillatory; at a distance less than the solvent diameter the attractive depletion force dominates the electrostatic repulsion. At a distance larger than a few solvent diameters, only the electrostatic repulsive forces govern the intermicellar interactions.

**5.2. Micelles in the Bulk Solution.** Typical radial distribution functions of the bulk micellar solution at the conditions that correspond to both low and high surfactant concentrations are shown in Figure 4. The main differences between two curves for high and low surfactant concentrations concern the positions of the maxima and minima and the magnitudes of the oscillations. In the case of high surfactant concentration the location of the first maximum is found at about 2 times the micelle hard-



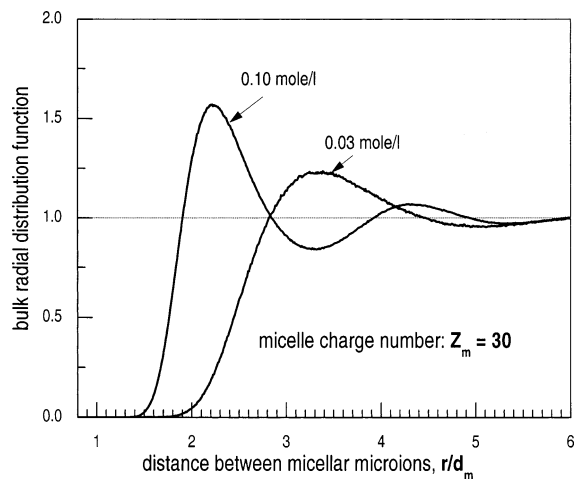


**Figure 4.** Monte Carlo data for the radial distribution function between micellar particles in a bulk solution. The low (0.03 mol/L) and high (0.10 mol/L) surfactant concentration conditions have been simulated. These correspond to micellar particle volume fractions  $\eta_m = 0.012$  and 0.050, respectively. The micellar charge number is fixed at  $Z_m = 30$  in both cases.

core diameter ( $r \approx 2d_m$ ) whereas for the low surfactant concentration the first maximum is shifted toward large distances and found to be at more than 3 times the hard-core micelle diameter ( $r \approx 3.3d_m$ ). This is an expected result and usually is interpreted as an increase of the effective micellar diameter (composed of the micelle hard core and the Debye atmosphere about the micelle) with a decrease in a surfactant concentration: at low surfactant concentration the total amount of simple ions in the solution is less and the Debye length according to eq 1 is larger. The amplitude of the oscillations is related to the micellar concentration itself: with an increase in surfactant concentration more micelles are present in solution. As a result of the increased micellar volume fraction, the first maximum of the radial distribution function at surfactant concentration  $C = 0.10$  mol/L is higher than the corresponding maximum at lower surfactant concentration,  $C = 0.03$  mol/L.

To illustrate how the distribution of the micelle particles in the bulk region is affected by the number of charges carried by particles, we show in Figure 4b the Monte Carlo data for two additional values of micellar charge number, namely,  $Z_m = 10$  and 20, maintaining in both cases the same value of  $\kappa$  that corresponds to high surfactant concentration (see Table 1). For comparison, on the same figure we show (the thin solid line) the micellar radial distribution functions that have been generated from Monte Carlo simulations using a Hamiltonian with only entropic forces that correspond to the limiting case where  $Z_m \rightarrow 0$ . Indeed, we observe that entropic and electrostatic forces are acting on different distance scales: in the close neighborhood of the micelles (entropic forces) or on the intermediate to large distances between them (electrostatic forces). The impact of these forces on the radial distribution function is different and depends on the volume fraction of micellar particles and the strength of electrostatic interaction between them. In practice, both of these factors are controlled by surfactant concentration. Lowering the surfactant concentration decreases the micellar volume fraction and moderates the electrostatic interaction. This results in a lower probability for the two micellar particles to approach each other and in a weakening of long-range ordering imposed by electrostatic forces (see Figure 5). In the case where the number of charges carried by micellar macroions is larger, e.g.,  $Z_m = 30$ , the entropic contribution to the effective pair interaction becomes irrelevant for the bulk radial distribution

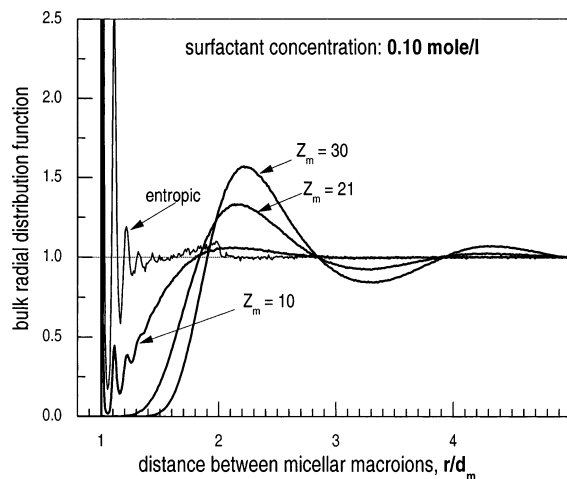


**Figure 5.** Monte Carlo data for the radial distribution function between micellar particles in a bulk solution at high (0.10 mol/L) surfactant concentration and different micellar charge numbers as depicted in the figure. The thin solid line shows Monte Carlo data obtained with entropic forces only, i.e.,  $Z_m = 0$ .

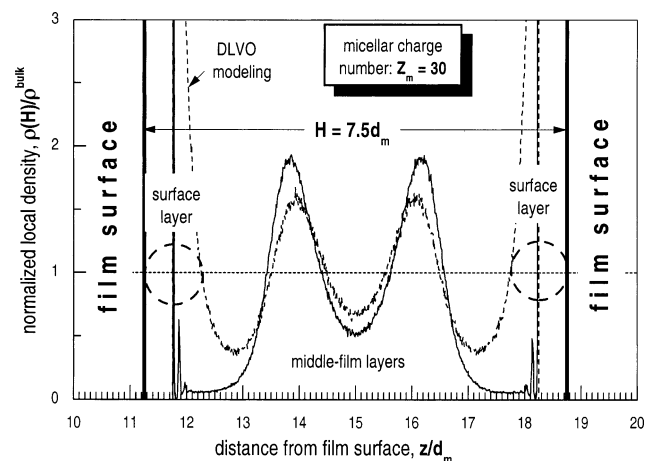


**Figure 6.** Monte Carlo data for the normalized local density distribution of the micellar particles in a film formed at high (0.10 mol/L) surfactant concentration. The thick vertical lines mark the film boundaries, i.e.,  $z_{\text{left}}$  and  $z_{\text{right}}$ , for different film thicknesses. The film contains four particle layers and has the thickness that corresponds to seven and half hard-core micellar diameters, i.e.,  $H = 7.5d_m$ . The dashed line shows the Monte Carlo data obtained from the simulation with electrostatic (DLVO) forces only. The micellar charge number is fixed at  $Z_m = 30$  in both cases.

functions (at least for considered range of the surfactant concentration): flocculation of micellar macroions in a bulk solution becomes energetically unfavorable and only electrostatic forces operate. As a consequence, even at low surfactant concentration, the micellar macroions show an ordering with the nearest neighbors positioned at  $r \approx 3d_m$ .

**5.3. Films Formed from Micelles.** The subject of main interest in the present study is the layer structuring in films formed from like-charged particles. Figures 6–9 show Monte Carlo data for the local density distribution of micellar particles across the model micellar films of different thicknesses. The common feature of these films is that each of them is in a “metastable” state; i.e., the thickness of each film is adjusted to produce the local minima in the configurational potential energy of the whole (bulk reservoir plus film region) simulated system. We find that for such conditions each of the films is composed of an integer number of particle layers. Namely, we see four layers for the film thickness shown in Figures 6 and 7; three and two layers in Figures 8 and 9. The film of each

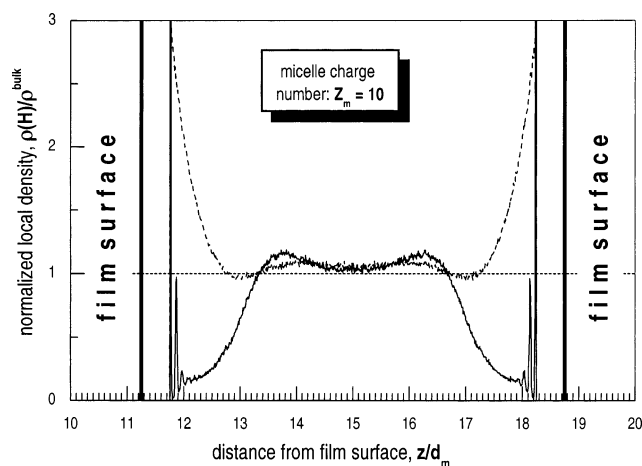


**Figure 7.** Same as in Figure 6 but with the micellar charge number fixed at  $Z_m = 10$  in both cases.

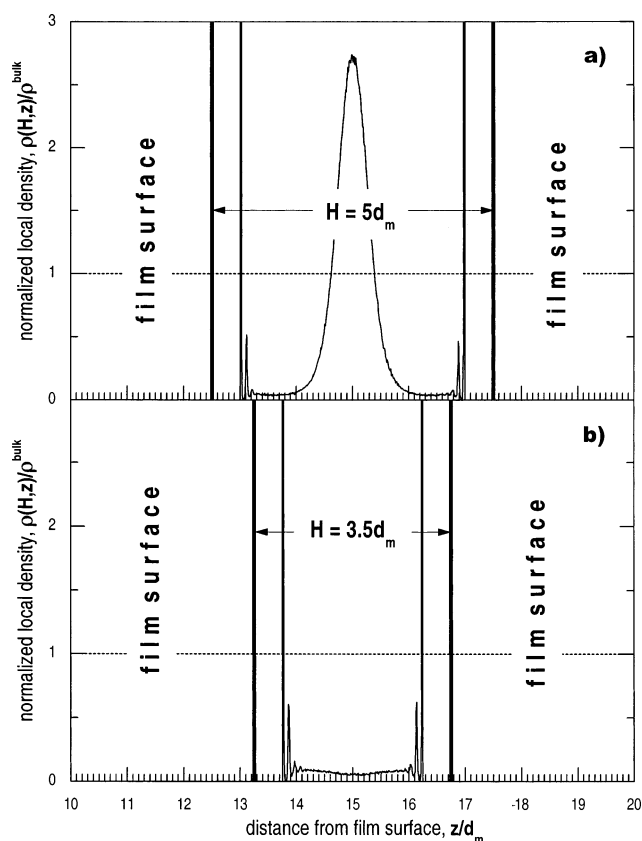


**Figure 8.** Monte Carlo data for the normalized local density distribution of the micellar particles in a film formed at high (0.10 mol/L) surfactant concentration. (a) The film contains three particle layers and has the thickness that corresponds to five hard-core micellar diameters, i.e.,  $H = 5d_m$ . (b) The film contains two surface particle layers and has the thickness that corresponds to three and one-half hard-core micellar diameters, i.e.,  $H = 3.5d_m$ . The micellar charge number is fixed at  $Z_m = 30$  in both cases.

thickness has been formed under controlled thermodynamic conditions ensured by the equilibrium with the rest of simulation cell, i.e., with bulk reservoir maintained at one of two micellar volume fractions that correspond to high or low surfactant concentration.

Figure 6 is used to introduce the notations and terminology that will help us to provide the discussion. The solid lines in Figures 6–9 display the main results of our calculations: Monte Carlo data for the normalized (with respect to the bulk region) local density distribution of micellar macroions across the film

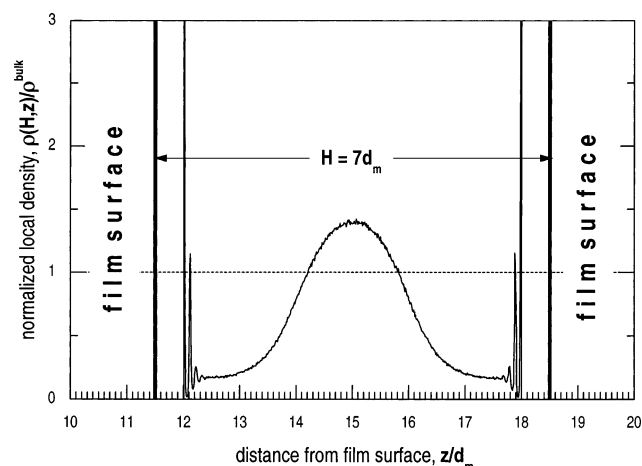


**Figure 9.** Monte Carlo data for the normalized local density distribution of the micellar particles in a film formed at low (0.03 mol/L) surfactant concentration. The film contains three particle layers and has the thickness that corresponds to seven hard-core micellar diameters, i.e.,  $H = 7d_m$ . The micellar charge number is fixed at  $Z_m = 30$ .

of thickness  $H$  that is scaled by the micelle hard-core diameter. These data are obtained from the simulations of the HS/SC/OCF model that, according to eq 5, incorporates both the electrostatic DLVO forces and entropic forces. To reveal the role that each of these forces is playing, Figures 6 and 7 show, by the dashed lines, Monte Carlo data for the density distribution in films formed under the same bulk conditions but assuming that the micellar particles interact only via a screened Coulomb potential, i.e., these data correspond to the SC/OCF (or DLVO-like) model. Both models in Figures 6 and 7 show that the like-charged particles confined to a film with a thickness between seven-to-eight hard-core particle diameters ( $H = 7.5 d_m$  on the Figures 6 and 7) are organized into four well-defined layers. There is an evident difference between the layers next to the film surfaces and those in the middle of the film. Each surface layer is rather narrow with the higher density of the particles condensed directly on the film surface steeply decreasing on going to the layer boundary. The particles in the middle region of the film could be considered as belonging to one middle-film superlayer that shows a tendency to separate into two middle-film layers. In contrast to the surface layers, the middle-film layers are thick and more diffusive. The thickness of each of the two middle-film layers in Figure 6 is around two hard-core micelle diameters whereas the surface layer thickness only slightly exceeds one hard-core diameter of micellar particles.

The main difference between the introduced HS/SC/OCF model and the DLVO-like models is found in the surface layers. In the case of the HS/SC/OCF model the surface layers themselves show a structuring with respect to the film surfaces. This results in each surface layer consisting of a well-defined sublayer in an immediate vicinity of the film surface and one or two similar sublayers that are less pronounced and are separated by an “effective” layer of a surfactant solution. The shape of the density profiles of the surface sublayers in the case of the SC/HS/OCF model has a  $\delta$ -like form, indicating that surface sublayers are the quasi-two-dimensional monolayers. The surface layers formed within the DLVO-like model, though thinner than the middle-film layers, still are far from being monolayers. As a result, the separation of the middle-film particle layers from the surface layers is not observed in this case. For the middle-film layers formed within the HS/SC/OCF and the DLVO-like models only some quantitative differences in the particle local density distribution are observed.



The micellar charge for the data presented in Figure 6 was fixed at  $Z_m = 30$ . As we learned from Figure 5, the role playing by entropic forces in the particle distribution in a bulk increases and becomes essential by reducing the micellar charge number. Figure 7 shows data identical to those in Figure 6 but assuming that the micellar charge number is smaller, i.e.,  $Z_m = 10$ . First of all we observe that the layering in the middle region of the film becomes less pronounced when electrostatic repulsion between particles becomes weaker. Second, the separation of the middle-film layers from the surface layers decreases. These trends are indicated qualitatively by both the HS/SC/OCF and SC/OCF models and have been observed already by González-Mozuelos et al.<sup>23,24</sup> in their DLVO-based study of the highly charged colloidal particles inside a charged planar slit. However, a further decrease in the number of charges carried by micellar particles causes more differences between two models. Particularly, in the limiting case  $Z_m \rightarrow 0$ , i.e., for a film formed by a hard-sphere fluid, two models differ substantially, as has been discussed recently.<sup>14,28</sup>

The evolution of micelle film structuring when a film becomes thinner has been studied in our simulations with the step  $\Delta H$  equal to  $1/10$ th of the particle hard-core diameter. We find that the next two films that provide the local minima of the potential energy (per film particle) have thicknesses around five and three particle hard-core diameters, respectively. Particularly, the film shown in Figure 8a has thickness  $H = 5d_m$  and contains three layers of micellar particles, i.e., has one layer less than the film discussed in Figure 6. Again we observe that the middle-film layer is almost completely separated from the surface layers. The thickness of the middle-film layer decreases slightly when the separation between film surfaces declines. In contrast, the surface layers do not change notably. This quasi-stability of the surface layers becomes even more evident by analyzing the local density distribution in the film that has a thickness around 3 times micelle hard-core diameter,  $H = 3.3d_m$ , and contains two surface layers only (see Figure 8b). We conclude that the surface layers for the three considered films remain largely unaffected and are almost identical.

The films discussed in Figures 6–8 are formed from the surfactant micelles at a high bulk surfactant concentration,  $C = 0.10$  mol/L. The effect of the decrease in surfactant concentration can be seen from Figure 9. Although for both surfactant concentrations the qualitative features of the particle layering are quite similar, two important trends with decreasing in surfactant concentration are observed from the comparison between Figures 8a and 9. The main changes are concerned with the middle-film region: the particle layering in the middle region of the films become less pronounced and a middle-film layer grows in its thickness. The thickness of the surface layers practically does not change, however, the particle density in the surface monolayer decreases. As a result, the total thickness of the films with the same number of particle layers is smaller when the surfactant concentration in the bulk is getting lower. In particular, the thickness of the film composed of three particle layers at a high surfactant concentration (Figure 8a) is five micelle hard-core diameters, whereas, for the low surfactant concentration (Figure 9), a similar thickness is seven micelle hard-core diameters.

**5.4. Relation to the Experiment.** Let us assume that during the film thinning process the film changes its thickness by squeezing out one layer of micelles. Then the height of the stepwise layer-by-layer thinning will depend on the effective thickness of the squeezed layer. To verify this assumption, the effective thicknesses of the squeezed layers have been calculated

**TABLE 2: Values of the Film Thickness,  $h_n$ , at the Metastable States Determined From the Interferogram of Thinning SDS Film at the High Surfactant Concentration,  $C = 0.10$  mol/L<sup>1</sup> and the Computer Simulation Data for the Equilibrium Film Thicknesses,  $H_m$ , Containing an Integer Number  $m$  of Particle Layers<sup>a</sup>**

| observation                   |                    | modeling                    |                   |       |
|-------------------------------|--------------------|-----------------------------|-------------------|-------|
| no. of metastable states, $n$ | film thickness, nm | no. of particle layers, $m$ | film thickness nm | $d_m$ |
| 0                             | 16.2               | 2                           | 15.84             | 3.3   |
| 1                             | 26.3               | 3                           | 24.48             | 5.1   |
| 2                             | 35.9               | 4                           | 36.00             | 7.5   |

<sup>a</sup> Monte Carlo simulations are performed at the micellar particle bulk volume fraction,  $\eta_m \approx 0.049$  and micellar charge number,  $Z_m = 30$ .

as the difference between the metastable thickness of the films containing four and three, three and two particle layers for both the low and high surfactant concentrations and compared with observation for the heights of the thinning steps (see Table 2). The film containing two surface layers is mostly stable and its thickness corresponds to the final film thickness in the film thinning process at the surfactant concentrations considered in the present study. These also agree qualitatively well with the force measurements of Richetti and Kékicheff.<sup>10</sup> These authors measured the force between two crossed mica cylinders immersed into micellar CTAB solutions. The zeroes of the measured force can be compared with the metastable film thicknesses in our modeling. From the highest concentration ( $\eta_m = 0.073$ ) studied by Richetti and Kékicheff we can see that the zeroes of the force (see Figure 3 of ref 10) are at  $\sim 15$ ,  $\sim 25$ , and  $\sim 35$  nm. These results correlate well with our findings for metastable film thicknesses revealed both from the film thinning experiments and from the computer modeling (see Table 2).

For the low surfactant concentration case the difference in the film thickness between the films containing three and two micellar layers is about 15.8 nm. The experimentally observed height of the stepwise thickness transition is about 15.3 nm. For the high surfactant concentration the difference in the film thickness for the films with three and two micellar layers is about 8.6 nm (see Figures 8a and 9 and Table 2) whereas the experimentally observed height of the stepwise thickness transition is about 10.4 nm. The increased deviation between simulation predicted the film-thickness difference and the measured value of the stepwise thickness transition at a high surfactant concentration are probably due to the fact that our present model does not account for the contributions of the finite size of the electrolyte ions as well as the solvent molecules to the electrostatic part of an effective interaction between the pair of micellar macroions. Our model accounts for the contributions of the finite size of the electrolyte ions and the solvent molecules to the entropic interaction only.

Finally, for the high surfactant concentration Figures 10 and 11 depict the three-dimensional snapshots of the like charged particle structuring phenomenon in the model films of two different thicknesses, e.g., at  $H = 5d_m$  and  $3.5d_m$ , corresponding to the three and two particle layers, respectively. The snapshots reveal the differences in micellar concentration, micellar distribution, and ordering in the bulk and in the film regions. The micelles inside the film form a layered structure and it is more noticeable for the surface layers than for the middle-film layer. The average micellar concentration in the film region is higher than that in the bulk. For instance, for the film containing two micellar layers, the micelle volume fraction in the film is about 30% more than that in the bulk. The snapshots shown in

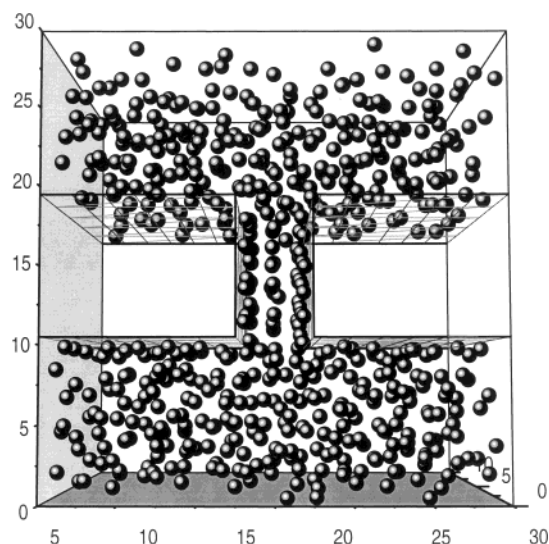


**Figure 10.** Snapshots of Monte Carlo generated configurations of micellar macroions at a bulk volume fraction,  $\eta_m = 0.049$ , which corresponds to a high surfactant concentration, 0.10 mol/L. The number of charges carried by micellar macroions,  $Z_m = 30$ . The film has a thickness of five hard-core micellar diameters, i.e.,  $H = 5d_m$ , and contains the three micellar layers: two surface layers plus one middle-film layer.

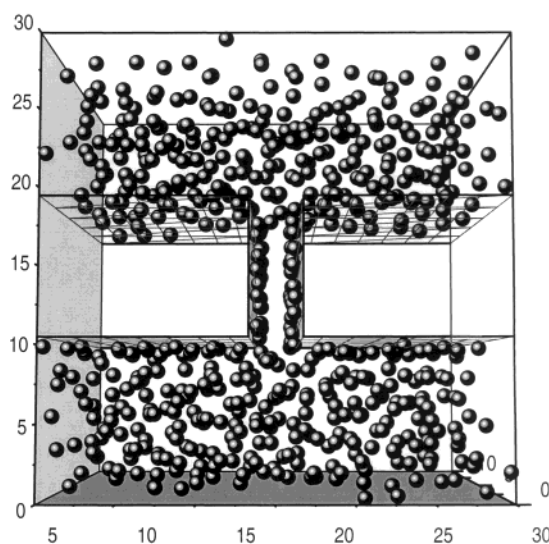


**Figure 11.** Same as in Figure 10 but for the film that has a thickness of three and one-half hard-core micellar diameters, i.e.,  $H = 3.5d_m$ , and contains two surface layers only.

these two figures as well as the local density curves shown in Figures 6–9 reveal that the middle-film layer is less dense and is less structured than the surface layers.

## 6. Concluding Remarks

The phenomenon of the layering of like-charged particles that form a thin liquid film between the two-plane surfaces is studied by applying the Monte Carlo simulation technique. The like-charged particles are used to mimic the ionic surfactant micelles whereas the plane surfaces model the air/water interfaces or rigid mica surfaces immersed in surfactant solution.

The results presented have been obtained from the simulations of a one-component fluid model with an effective pair potential that incorporates micellar hard-core repulsion, the screened Coulomb electrostatic interaction, and the entropic forces due to the discrete nature of the solvent and a finite size of electrolyte

ions. The potential of an effective interaction between a pair of micellar particles has been evaluated within the ion–dipole model of electrolyte solutions using the mean-force-potential methodology, i.e., from the radial distribution function between the two macroions in the limit of their infinite dilution.

We find that the HS/SC/OCF and SC/OCF models differ in quantitative implementation of the layering phenomena. The most evident difference is concerned with the surface layers: for the HS/SC/OCF model, due to the entropy-induced attraction between micellar particles and film surfaces, the surface layers are practically monolayers whereas for the SC/OCF model, with the electrostatic repulsion only, the surface layers are diffuse. Although the increase of the micellar charge number will cause the reordering within the particles belonging to the surface layer exclusively due to the electrostatic pressure exerted by the unconfined particles on the adsorbed particles,<sup>23,24</sup> the entropic forces play an important role in the organization of the surface layer. In general, the entropic forces are more important for the higher densities and this is a case of particle layers, both near the surface and in the middle of the film. Summarizing, the electrostatic forces in micellar solutions play a crucial role in the well-defined layering whereas the entropic forces could contribute to the local ordering inside a layer.

The effects of the micellar volume fraction (or surfactant concentration) on the micelle layering versus film thickness and particularly on the evolution of the layering structure within the film were analyzed and discussed. The computer simulation data have confirmed the suggestion raised from observations that as a result of the film confinement the micelles (or any other like-charged colloidal particles) form layers parallel to the film surfaces. At high particle concentrations the layered structure is improved. It was found that the phenomenon of particle structuring is governed by the electrostatic repulsion between the ionic micelles under the conditions of two-surface confinements and the depletion attraction between micelles and film surfaces. As a result, two types of layers have been observed: surface layers and middle-film layers. The surface layers are more dense and well structured; the middle-film layers are less packed and diffusive. The heights of the film stepwise thinning for two different surfactant concentrations were estimated and found to be in reasonable agreement with the experimentally observed data.

For both the low and high surfactant concentrations the surface layers are more dense than the middle-film layer. The thickness of the surface layer is approximately one micellar hard-core diameter (e.g., the micelle density profile in the vicinity of a film surface has a  $\delta$ -like shape that indicates that the thickness of the surface layer only slightly exceeds the one micellar hard-core diameter). Due to the presence of the charges on the micellar surface, the micelle is surrounded by the Debye atmosphere, and consequently, the micelle effective diameter is larger than its actual hard-core diameter ( $d_m = 4.8$  nm). The effective micelle diameter includes the micelle hard-core diameter plus the layers of the solvent molecules and simple electrolyte ions surrounding the micelle (e.g., see the two small oscillations in the inner part of the normalized local density curves in Figures 6–9). Therefore, the film containing three micellar layers has a thickness greater than three micellar hard-core diameters. The oscillatory decay depicts the ability of the supporting electrolyte (due the discrete nature) to form layers around the micelles.<sup>1</sup>

The simulation data reported in this study partially support the “squeezing layer” mechanism. The snapshots shown in Figure 11 clearly indicate that the middle-film layer is much

less organized and the average intermicellar distance inside this layer is larger than the intermicellar distance inside the surface layer. However, to discuss more accurately the conditions of the squeezing mechanism inside the middle-film layer, the effect of the film thickness on the in-layer micellar structure should be considered. Also, the effects of the charges on the film surfaces should be analyzed as well. These efforts are currently undertaken in our laboratory.

**Acknowledgment.** This study was supported in part by the National Science Foundation (Grants No. CHE 98-13729 and CTS 01-00854) and the Department of Energy under Grant No. DE-FG07-97ER14828.

## References and Notes

- (1) Nikolov, A. D.; Wasan, D. T. *J. Colloid Interface Sci.* **1989**, *133*, 1.
- (2) Nikolov, A. D.; Wasan, D. T.; Denkov, N. D.; Kralchevsky, P. A.; Ivanov, I. B. *Prog. Colloid Polym. Sci.* **1990**, *82*, 87.
- (3) Basheva, E. S.; Nikolov, A. D.; Kralchevsky, P. A.; Ivanov, I. B.; Wasan, D. T. *Surfactants Solution* **1991**, *11*, 467.
- (4) Nikolov, A. D.; Wasan, D. T. *Langmuir* **1992**, *8*, 2985.
- (5) Wasan, D. T.; Nikolov, A. D.; Lobo, L. A.; Koczko, K.; Edwards, D. A. *Prog. Surf. Sci.* **1992**, *39*, 119.
- (6) Koczko, K.; Nikolov, A. D.; Wasan, D. T.; Borwankar, R. P.; Gonsalves, A. J. *J. Colloid Interface Sci.* **1996**, *178*, 694.
- (7) Nikolov, A. D.; Kralchevsky, P. A.; Ivanov, I. B.; Wasan, D. T. *J. Colloid Interface Sci.* **1989**, *133*, 13.
- (8) Kralchevsky, P. A.; Nikolov, A. D.; Wasan, D. T.; Ivanov, I. B. *Langmuir* **1990**, *6*, 1180.
- (9) Bergeron, V.; Radke, C. J. *Langmuir* **1992**, *8*, 3020.
- (10) Richetti, P.; Kélicheff, P. *Phys. Rev. Lett.* **1992**, *68*, 1951.
- (11) Wasan, D. T.; Nikolov, A. D. In *Supramolecular in Confined Geometries*; Manne, S., Warr, G., Eds.; ACS Symposium Series No. 736; American Chemical Society, 1999; p 40.
- (12) Chu, X. L.; Nikolov, A. D.; Wasan, D. T. *Langmuir* **1994**, *10*, 4403.
- (13) Chu, X. L.; Nikolov, A. D.; Wasan, D. T. *J. Chem. Phys.* **1995**, *103*, 6653.
- (14) Trokhymchuk, A.; Henderson, D.; Nikolov, A.; Wasan, D. J. *Colloid Interface Sci.* **2001**, *243*, 116.
- (15) Wasan, D. T.; Nikolov, A. D. In *Particulate Two-Phase Flow*; Roco, M. C., Ed.; Butterworth-Heinemann: London, 1993; p 325.
- (16) Chu, X. L.; Nikolov, A. D.; Wasan, D. T. *Chem. Eng. Commun.* **1996**, *148–150*, 325.
- (17) Chu, X. L.; Nikolov, A. D.; Wasan, D. T. *Langmuir* **1996**, *12*, 5004.
- (18) Xu, W.; Nikolov, A. D.; Wasan, D. T. *AIChE J.* **1997**, *43*, 3215.
- (19) McMillan, W. G.; Mayer, J. E. *J. Chem. Phys.* **1945**, *13*, 276.
- (20) Vlachy, V. *Annu. Rev. Chem.* **1999**, *50*, 145.
- (21) Valdez, M. A.; Manero, O. J. *Colloid Interface Sci.* **1987**, *189*, 230.
- (22) González-Mozuelos, P.; Medina-Noyola, M. J. *J. Chem. Phys.* **1991**, *94*, 1480.
- (23) González-Mozuelos, P.; Alejandre, J.; Medina-Noyola, M. J. *J. Chem. Phys.* **1991**, *95*, 8337.
- (24) González-Mozuelos, P.; Alejandre, J.; Medina-Noyola, M. J. *J. Chem. Phys.* **1992**, *97*, 8712.
- (25) Pollard, M. L.; Radke, C. J. *J. Chem. Phys.* **1994**, *101*, 6979.
- (26) Dijkstra, M.; van Roij, R.; Evans, R. *Phys. Rev. Lett.* **1999**, *82*, 117.
- (27) Dijkstra, M.; van Roij, R.; Evans, R. *Phys. Rev. E* **1999**, *59*, 5744.
- (28) Trokhymchuk, A.; Henderson, D.; Nikolov, A.; Wasan, D. T. *Phys. Rev. E* **2001**, *64*, 012401.
- (29) Reiss-Husson, F.; Luzzati, V. *J. Phys. Chem.* **1964**, *68*, 3504.
- (30) Sasaki, T.; Hattori, M.; Sasaki, J.; Nukina, K. *Bull. Chem. Soc. Jpn.* **1975**, *48*, 1397.
- (31) Hartley, G. S. *Aqueous Solutions of Paraffin-Chain Salts*; Hermann: Paris, 1936.
- (32) Derjaguin, B.; Landau, L. *Acta Phys. Chim. URSS* **1941**, *14*, 633.
- (33) Verwey, E. J. W.; Overbeek, J. Th. G. *Theory of the Stability of Lyophobic Colloids*; Elsevier: Amsterdam, 1948.
- (34) Sogami, I.; Ise, N. *J. Chem. Phys.* **1984**, *81*, 6329.
- (35) Spalla, O.; Belloni, L. *Phys. Rev. Lett.* **1995**, *74*, 2515.
- (36) Ise, N.; Smalley, M. V. *Phys. Rev. B* **1994**, *50*, 16722.
- (37) Ito, K.; Yoshida, H.; Ise, N. *Science* **1994**, *263*, 66.
- (38) Larsen, A. E.; Grier, D. G. *Nature* **1997**, *385*, 230.
- (39) Crocker, J. C.; Grier, D. G. *Phys. Rev. Lett.* **1996**, *77*, 1897.
- (40) Israelachvili, J. N. *Intermolecular and Surface Forces*, 2nd ed.; Academic Press: London, 1992.
- (41) Vericat, F.; Blum, L. *J. Stat. Phys.* **1980**, *22*, 593.
- (42) Holovko, M. F.; Trokhymchuk, A.; Protsykevich, I.; Henderson, D. *J. Stat. Phys.* **1993**, *72*, 1391.
- (43) Trokhymchuk, A.; Henderson, D.; Wasan, D. J. *Colloid Interface Sci.* **1999**, *210*, 320.
- (44) Trokhymchuk, A.; Holovko, M. F.; Henderson, D. *Mol. Phys.* **1993**, *80*, 1009.
- (45) Henderson, D. *J. Colloid Interface Sci.* **1988**, *121*, 486.
- (46) Asakura, S.; Oosawa, J. *J. Chem. Phys.* **1954**, *22*, 1255.
- (47) Henderson, D.; Lozada-Cassou, M. J. *Colloid Interface Sci.* **1986**, *114*, 180.
- (48) Mao, Y.; Cates, M. E.; Lekkerkerker, H. N. W. *Physica* **1995**, *A 222*, 10.
- (49) Roth, R.; Evans, R.; Dietrich, S. *Phys. Rev. E* **2000**, *62*, 5360.
- (50) Trokhymchuk, A.; Henderson, D.; Nikolov, A.; Wasan, D. T. *Langmuir* **2001**, *17*, 4940.
- (51) Blum, L.; Høye, J. S. *J. Chem. Phys.* **1977**, *81*, 1311.
- (52) Lee, E. M.; Simister, E. A.; Thomas, R. K.; Penfold, J. *Colloid Phys.* **1989**, *50*, 75.
- (53) Adams, D. J. *Mol. Phys.* **1979**, *37*, 211.
- (54) van Megen, W.; Snook, I. K. *J. Chem. Phys.* **1980**, *72*, 2907.
- (55) Gao, J.; Luedtke, W. D.; Landman, U. *J. Phys. Chem. B* **1997**, *101*, 4013.
- (56) Gao, J.; Luedtke, W. D.; Landman, U. *J. Chem. Phys.* **1997**, *106*, 4309.
- (57) Gao, J.; Luedtke, W. D.; Landman, U. *Phys. Rev. Lett.* **1997**, *79*, 705.
- (58) Spohr, E.; Trokhymchuk, A.; Henderson, D. *J. Electroanalytical Chem.* **1998**, *450*, 281.
- (59) Kaluzhnyi, Yu. V.; Stell, G.; Llano-Restrepo, M. L.; Chapman, W. G.; Holovko, M. F. *J. Chem. Phys.* **1994**, *101*, 7939.
- (60) Trokhymchuk, A.; Pizio, O.; Henderson, D.; Sokolowski, S. *Mol. Phys.* **1996**, *88*, 1491.